

# Development of a Nanoscale DNA Based Force Transducer

Michael W. Hudoba, Carlos E. Castro

## Introduction

Biological cells navigate their environment by exerting a field of traction forces applied via a multitude of localized attachment points to the surrounding extracellular matrix termed focal adhesion sites. During cellular migration, the cell cytoskeleton protrudes forward in the direction of motion, adheres to the extracellular matrix, and then applies contractile forces at these adhesion sites to pull the body of the cell forward (figure 1). Different cells have been shown to exhibit different traction force fields during migration<sup>1-5</sup>, and understanding these cellular traction forces (CTF) at the molecular scale can allow scientists to engineer systems to manipulate cell migration, for example for cell separation. This research aims to improve upon existing methods of traction force measurement by developing a nanoscale molecular force transducer (NMFT) using a process known as DNA origami. Scaffolded DNA origami is a process of folding single stranded DNA (ssDNA) into 2 and 3 dimensional shapes via molecular self-assembly. The NMFTs will improve upon current CTF measurements by improving resolution (piconewton force resolution with nanometer spatial resolution), and by enabling measurement of single molecule force interactions in a physiologically realistic 3 dimensional environment.

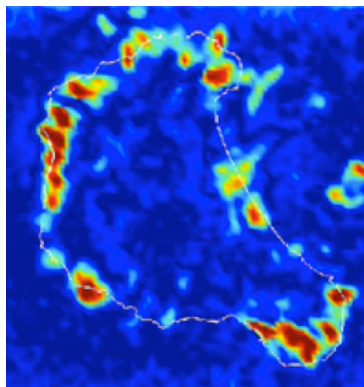


Figure 1 – Field of traction forces (cell body outlined in white) [Gardel Lab, University of Chicago]

Currently, there are two widely used methods for measuring CTFs. The first, known as cellular traction force microscopy (CTFM), utilizes microbeads imbedded in a soft substrate to measure local deflections of the substrate after a cell has applied contractile forces. The left and right images in figure 2 show examples of 2 and 3 dimensional CTFM, respectively. In the left image an arrow shows the direction of cell migration, and the white dots are fluorescently labeled beads imbedded within the polyacrylamide cell substrate. In the right image, a cell (shown in blue) is embedded in a polyacrylamide gel seeded with red tracker particles. The fluorescent beads and tracker particles are used to measure deformation as a result of the forces being exerted by the cell. Knowing the mechanical properties of the substrate, these local deformations can be used to find a field of traction forces<sup>1,2,3</sup>. The second approach uses array of micro or nanopillars, which act like cantilevered beams that deflect under applied cellular forces<sup>4,5</sup> (figure 3). The cantilever deflections can then be used to calculate applied cellular forces.

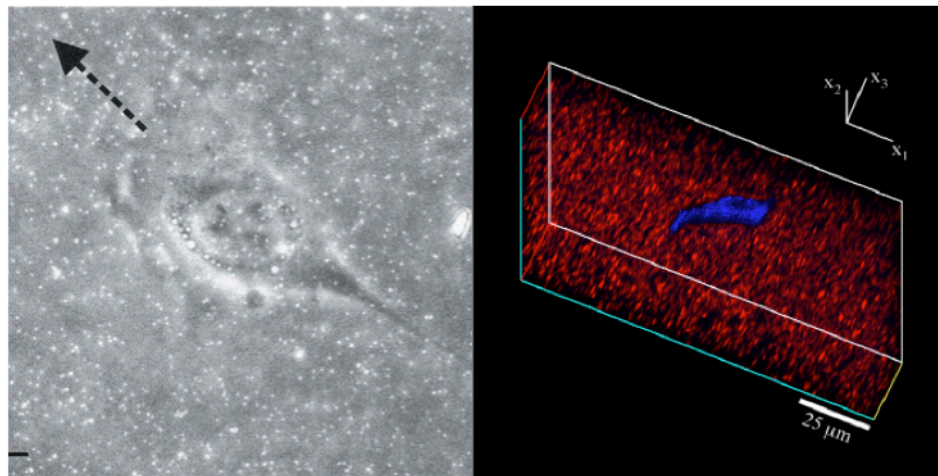


Figure 2 – 2D (left)<sup>2</sup> and 3D (right)<sup>3</sup> Traction Force Microscopy

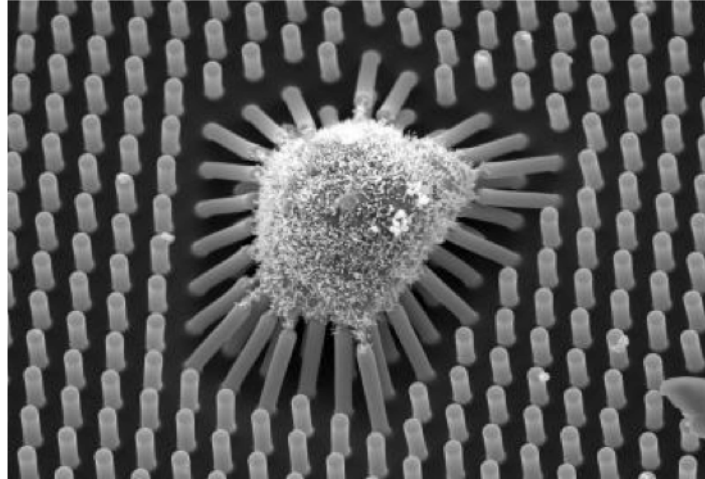


Figure 3 – Deflection of Micropillar Array

Both methods have inherent drawbacks and limitations. First, they are generally limited to 2D migration studies, whereas the physiological cellular environment is typically a 3D fibrous environment. 3D CTFM has been demonstrated<sup>3</sup>; however, this has only been implemented in non-physiological hydrogel materials. Second, with these methods cellular forces are not measured directly, but instead deflections of beads or pillars are measured and converted into forces. This requires knowledge of the substrate or pillar mechanical properties and some assumptions of the location of forces resulting in non-unique solutions. Furthermore, errors may be introduced through unintended substrate deflection. Finally, both approaches cannot measure forces transmitted at individual membrane proteins or individual focal adhesions, but instead measure a collective group of forces with a resolution of several 10's to 100's of piconewtons, far greater than the expected magnitude of individual contractile forces.

Our DNA based nanoscale force transducer is designed to measure individual contractile forces with  $\sim$ pN level resolution. These forces are directly measured via fluorescence resonance energy transfer (FRET) efficiency readouts. They are also designed so that they can be easily integrated into a 3D environment to study physiologically realistic cellular migration.

In addition to designing the NMFTs, a primary objective of this research is to use these devices to measure cellular migration of healthy and cancerous cells. Specifically, experiments will be implemented to study the migration patterns of healthy cells and U251 glioma cells (a highly invasive brain cancer) on flat and fibrous substrates. Ultimately, the differences in migration characteristics will be used to develop separation pathways for cell sorting.

### **DNA Origami**

DNA origami, developed in 2006 by Paul Rothemund, is a process used to create complex 2D and 3D nanostructures (figure 4) with typical dimensions of 10-100 nm and geometry controlled to ~1 nm spatial resolution<sup>6,7,8</sup>. Structures are made using a long (7000-8000 bases) ssDNA ‘scaffold’ strand derived from the M13MP18 bacteriophage viral genome, and many shorter ssDNA ‘staple’ strands (~50 bases) designed to be piece-wise complementary to the scaffold according to Watson-Crick base pairing<sup>7</sup>. During the self-assembly reaction the scaffold folds in order to spatially collocate regions of the scaffold that are complementary to individual staples in order to maximize base pairing as shown in figure 5. The scaffold and staples assemble into close-packed bundles of double-stranded DNA (dsDNA) helices. The sequences of the staples are designed so that these bundles arrange into the desired higher order structure. For the purposes of structural design, dsDNA helices are typically depicted as solid cylinders shown in figure 5.

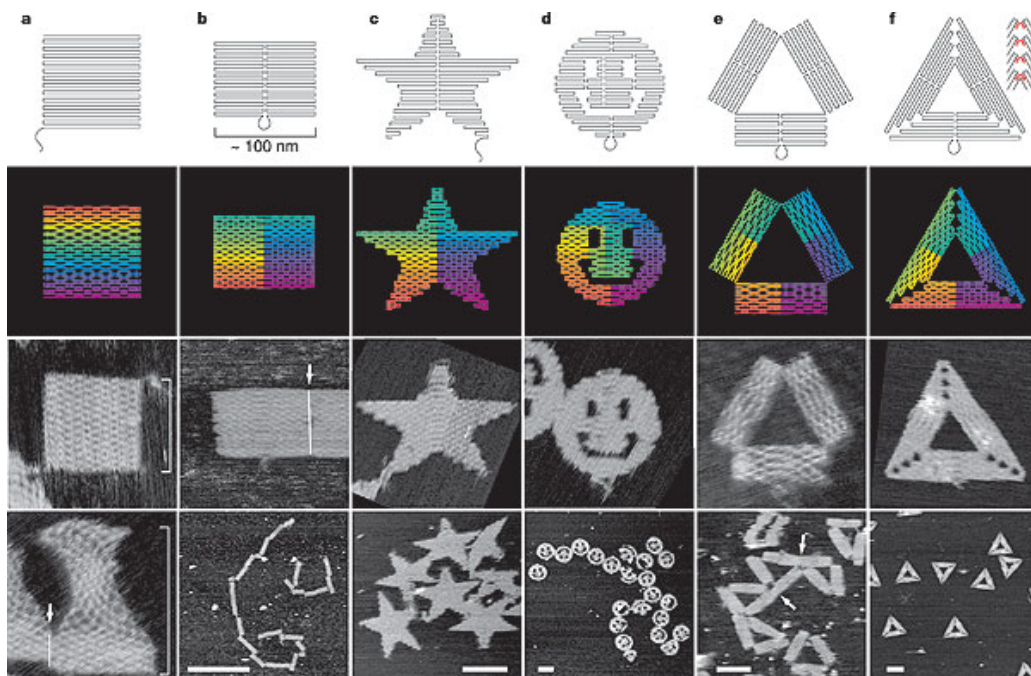


Figure 4 – Two-Dimensional DNA Origami

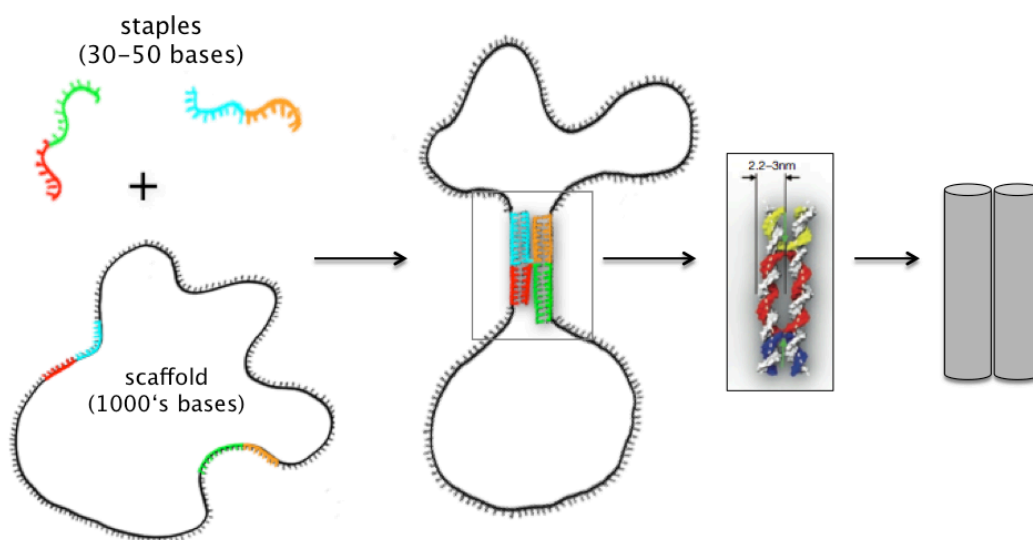


Figure 5 – DNA Origami and Design Representation

## Force Transducer Design

DNA origami was used to design and develop the NMFT shown in figure 6. The left image shows the schematic broken down into three modules. The NMFT consists of two handles connected by two curved bundles of DNA that can be thought of as mechanical springs. Module

1 enables specific attachment to a cell membrane via a ligand for a membrane bound receptor. Module 2 contains the mechanical springs and the Fluorescence Resonance Energy Transfer (FRET) readout for force measurement. Finally, module 3 enables specific attachment to a functionalized substrate. The DNA origami solid model of the NMFT is shown in the right of figure 6, where each cylinder is representative of a DNA double helix.

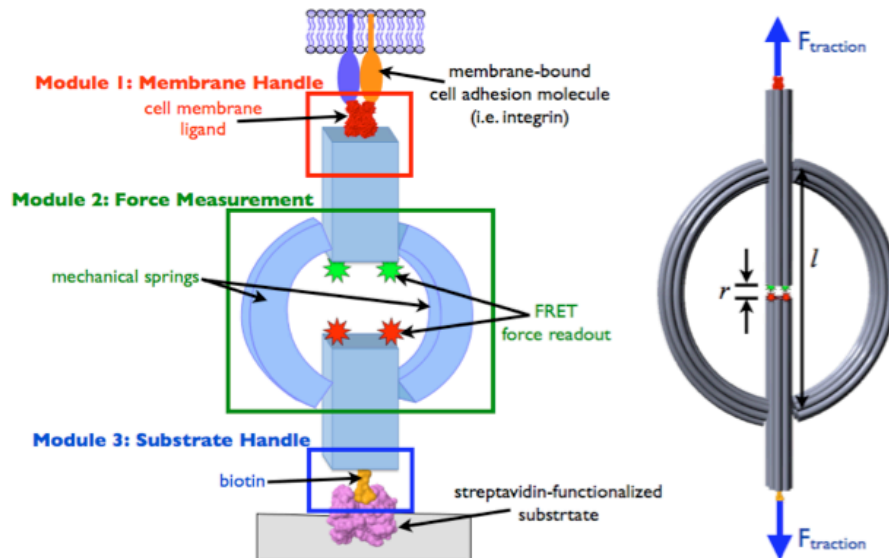


Figure 6 – NMFT schematic (left) and solid model (right)

The membrane and substrate handles (modules 1 and 3) can be functionalized for attachment by modifying specific staples at the outer end of each handle. A single staple is designed to present a ssDNA overhang where it is functionalized with biotin. The biotin functionality can attach to a streptavidin-functionalized substrate or fibronectin for modules 3 and 1, respectively.

Module 2, the force measurement module, is where deformation can be measured and converted into a force readout. In order to measure the force, it is critical to know the stiffness ( $K_B$ ) of the curved bundles of DNA, and we must have an accurate way of measuring the separation distance ( $r$  in figure 6) of the inner ends of the two handles.

FRET is used to measure the separation distance  $r$ . FRET is a process that uses two fluorescent dyes known as a FRET pair. The first dye (donor, green) excites at a lower wavelength than the second dye (acceptor, red). When a fluorescent dye is excited, that energy is absorbed and emitted at a slightly higher wavelength light, which can then be absorbed and emitted by the acceptor dye causing a further shift to larger wavelengths. The efficiency of energy transfer between donor and acceptor (FRET efficiency,  $E_t$ ) can be correlated to the separation distance between the FRET pair as shown in figure 7. In the NMFT, the donor and acceptor dyes were positioned at the inner ends of the handles by addition of the fluorescent dye to the appropriate staple base.

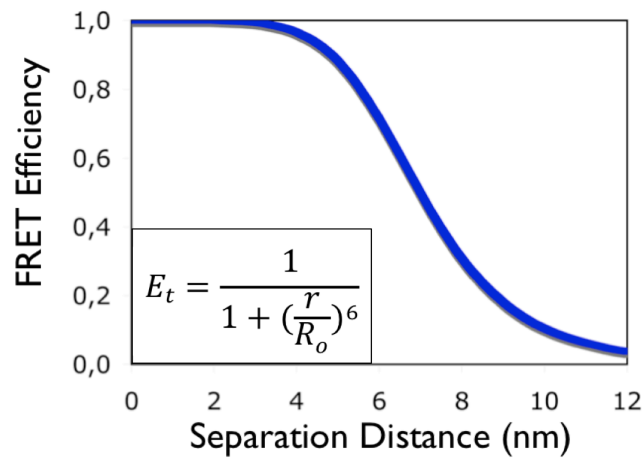


Figure 7 – FRET Efficiency versus Separation Distance

The NMFT is designed so at no force the handles are  $\sim 2$  nm apart from one another, resulting in a high FRET efficiency (see figure 7). As force is applied to the outer ends of the handles, the curved beams begin to unbend, which separates the fluorescent dyes resulting in a lower FRET efficiency. Equation 1 relates the measured FRET efficiency to the theoretical relationship given in figure 7. By measuring the intensity of the donor ( $I_D$ ) and acceptor ( $I_A$ ), equation 1 one can be used to find  $r$ , the separation distance ( $R_o$  is a factor corresponding to the



specific FRET pair being used, and  $\beta$  is a correction factor that accounts differences in detection efficiencies and background).

$$E_t = \frac{I_A}{I_A + \beta I_D} = \frac{1}{1 + (\frac{r}{R_o})^6} \quad (1)$$

The relationship between FRET efficiency and applied force is dependent upon the stiffness  $K_B$  of the curved beams. Using a small strain approximation of the curved beam gives the  $K_B$  shown in equation (2), where  $EI$  is the bending stiffness of the bundle,  $\rho$  is the arc radius, and  $\alpha$  is the arc angle<sup>9</sup>. Figure 8 shows the geometry and cross section of the NMFT. The Young's Modulus ( $E$ ) of DNA has been experimentally characterized<sup>10</sup>, and the area moment of inertia ( $I$ ) of the cross section can be calculated using the parallel axis theorem.

$$K_B = \frac{EI}{\rho^3 \left[ \frac{1}{2} \alpha \left( 1 + \frac{1}{2} \cos(\alpha) \right) - \frac{3}{4} \sin(\alpha) \right]} \quad (2)$$

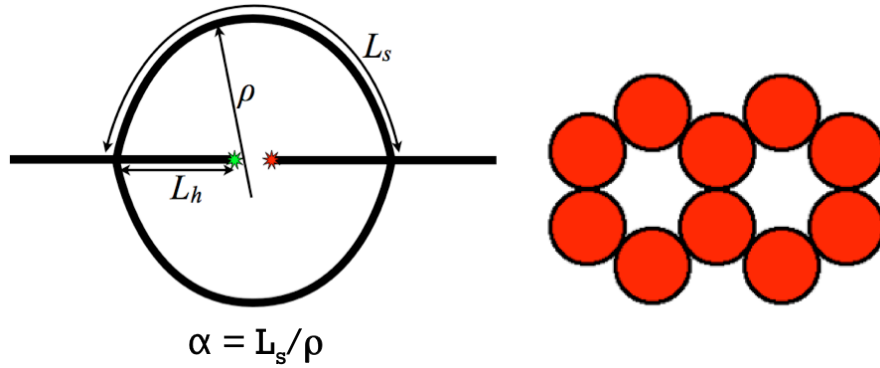


Figure 8 – NMFT Geometry (left) and cross section (right)

The arc angle and arc radius of the 10-helix bundle can be approximated during the design of the DNA origami structure. The backbone of each ssDNA in a dsDNA helix rotates  $720^\circ$  every 21 base pairs. Structures can achieve curvature by introducing base pair additions or deletions within this 21 base pair framework. If bases are added ( $>21$  base pairs/ $720^\circ$ ),



compression is introduced to that segment of dsDNA. If bases are subtracted ( $<21$  base pairs/ $720^\circ$ ), tension is introduced. If this process is done so that the helices on one half of the cross section are in compression and the helices of the other half of the cross section are in tension, the natural relaxed state of the bundle becomes curved. The degree of curvature ( $\rho$  and  $\alpha$ ) is dependent upon the number of additions and deletions. We calculated a theoretical bending stiffness  $K_{B,\text{design}} = 4.4$  pN/nm using the original design parameters  $\rho = 36$  nm,  $L_s = 75$  nm, and  $I = 77$  nm<sup>4</sup>.

### **Force Transducer Characterization**

Once the design was created with a theoretical bending stiffness of  $K_{B,\text{design}} = 4.4$  pN/nm, the structures were fabricated via molecular self-assembly according to protocols established in [Castro et al., Primer paper]. In short, the scaffold and staples were mixed with 1 mM EDTA, 5 mM Tris, 5 mM NaCl, and 18 mM MgCl<sub>2</sub>. This folding reaction was then subjected to a thermal annealing ramp. During the thermal ramp, the structures are initially heated up to a temperature of  $65^\circ$  to melt all of the dsDNA into their individual ssDNA components. Then, the solution is cooled on the time scale of days to allow for a slow, organized folding process. Figure 9 shows the schematic design of the NMFT along with transmission electron microscopy (TEM) images of the folded structures.

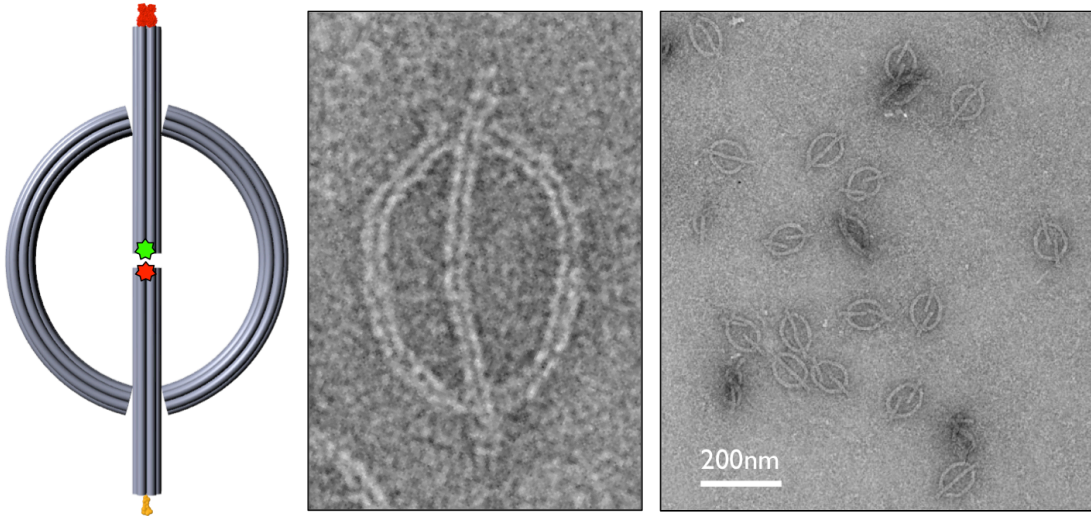


Figure 9 – Schematic (left) and TEM images (right) of the NMFT

In order to characterize the actual bending stiffness of the device we measured the end-to-end distance of the curved beam springs ( $l$ , figure 10) from TEM images for 226 NMFTs. Figure 10 shows a histogram of the distance  $l$ , with an average  $l = 68.4 \pm 1.4$  nm (S.D.). The width of this histogram is indirectly proportional to the bending stiffness. At the nanoscale, thermal fluctuations cause the springs to slightly bend and unbend, which translates to fluctuations in the end-to-end distance. For a stiffer device, these fluctuations would be small, decreasing the width of the histogram. From this information, the theorem of equipartition of energy (equation 3) was used to calculate an actual bending stiffness  $K_{B,\text{measured}} = 5.0$  pN/nm, very close to  $K_{B,\text{design}} = 4.4$  pN/nm.

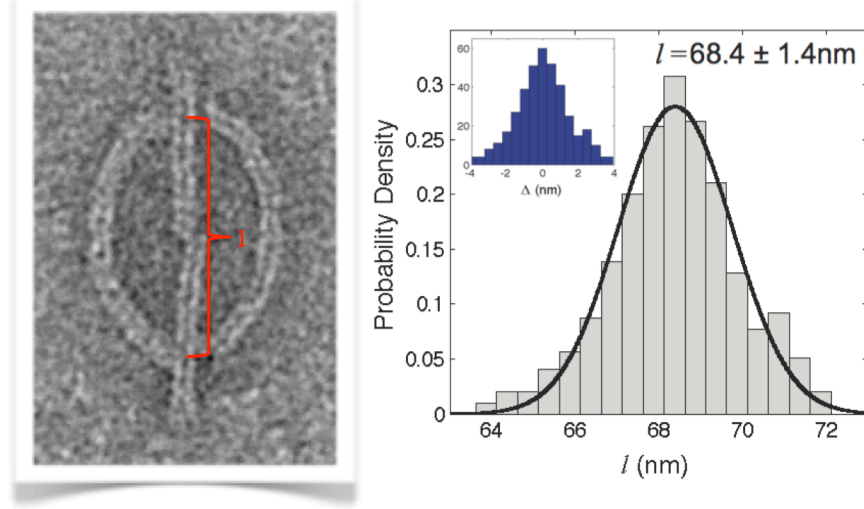


Figure 10 – Stiffness measurement of NMFT

$$U_{s_{ave}} = \frac{1}{2} K_B (\Delta^2)_{ave} = \frac{1}{2} K_B \langle (l - l_o)^2 \rangle = \frac{1}{2} k_B T \quad (3)$$

In order to predict the full force measurement range of the NMFT, we used a nonlinear force-extension model to describe the full unbending of the curved beams<sup>9</sup>. This model is given in equation 4. Equation 1 was manipulated to show the spring displacement ( $r$ ) in terms of FRET efficiency ( $e_{FRET}$ ), shown in equation 5. Finally, combining equations 2, 4, and 5 gives the resulting force/FRET relationship shown in equation 6 for the NMFT.

$$F = \frac{1}{2} K_B \left( l - l_0 - \frac{FL_s}{EA} \right) + EI \left[ 2\rho^2 \left( L_s - l + \frac{FL_s}{EA} \right) \right]^{\frac{2}{3}} \left( \frac{l - l_0 - \frac{FL_s}{EA}}{L_s - l_0} \right)^{2.5} \quad (4)$$

$$r = R_0 \left( \frac{1}{e_{FRET}} - 1 \right)^{\frac{1}{6}} - r_0 \quad (5)$$

$$F = \frac{1}{2} K_B \left( R_0 \left( \frac{1}{e_{FRET}} - 1 \right)^{\frac{1}{6}} - r_0 - \frac{FL_s}{EA} \right) + EI \left[ 2\rho^2 \left( L_s - R_0 \left( \frac{1}{e_{FRET}} - 1 \right)^{\frac{1}{6}} - r_0 - l_0 + \frac{FL_s}{EA} \right) \right]^{\frac{2}{3}} \left( \frac{R_0 \left( \frac{1}{e_{FRET}} - 1 \right)^{\frac{1}{6}} - r_0 - \frac{FL_s}{EA}}{L_s - l_0} \right)^{2.5} \quad (6)$$

## Preliminary Cellular Traction Force Experiments

The goal of the NMFT is to understand molecular mechanisms of force application during cellular migration by measuring cell traction forces at the single molecule or single focal adhesion scale. Initial experiments are being conducted to learn how cells migrate on glass surfaces. Figure 11 shows fluorescent images of cells attached to NMFTs on a glass surface. NMFTs were attached to a streptavidin functionalized glass coverslip. The other end of device was then functionalized with fibronectin to attachment sites for cellular adhesion. Prior to introducing cells, a blocking protein (casein) was introduced to block non-specific adhesion to glass. U251 glioma cells were then added and the cells adhered to the fibronectin end of the NMFTs. In figure 11, the left panel is direct imaging of the cell and the right two images show fluorescence, where each individual dot corresponds to a single NMFT. The center panel shows donor excitation and donor emission, while the right panel shows donor excitation, acceptor emission. FRET efficiency can be calculated by measuring the relative intensities of donor and acceptor dyes at the same spatial location.

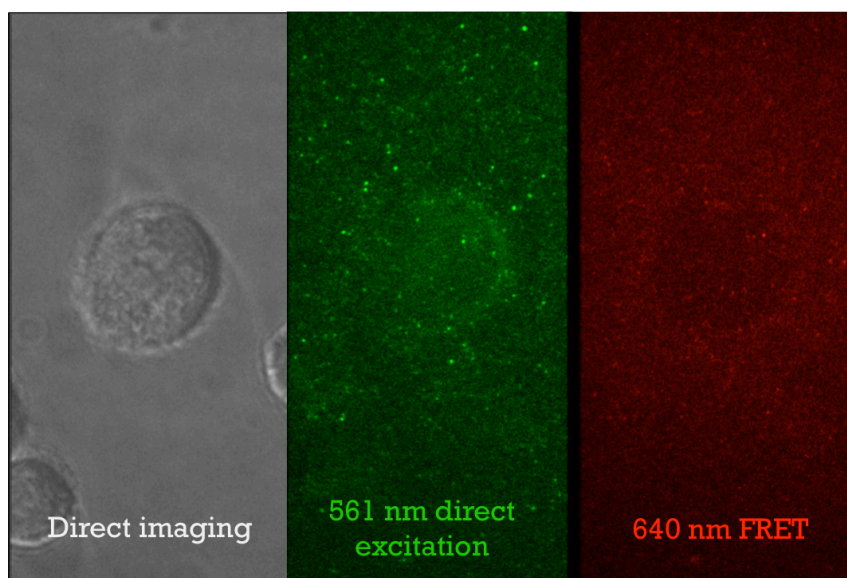


Figure 11 – Direct and fluorescent imaging of U251 Glioma cell line on NMFTs

In addition to studying migration patterns of cells on flat surfaces, we also have begun preliminary experiments to study cell migration on arrays of electrospun nanofibers. First, the structures were attached to the nanofibers by coating the nanofibers with streptavidin and allowing the biotin end of the NMFTs to adhere. Figure 12 shows TEM images of NMFT devices attached to nanofibers confirming specific attachment at one end of the device.

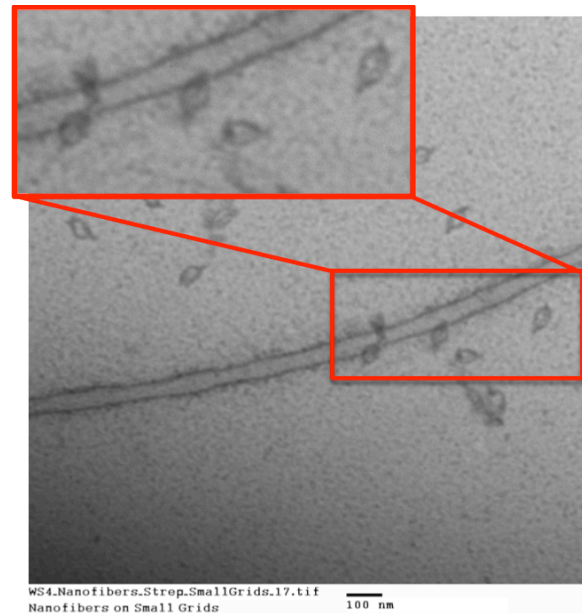


Figure 12 – TEM of NMFTs on electrospun nanofibers

Once we had confirmed attachment, we used fluorescence imaging to show the cells attached to the NMFT-nanofiber array. The left image of figure 13 shows the cells (U251 glioma cell line), fluorescently labeled with calcein, attached to the nanofiber array. The right half of figure 13 shows the fluorescence of the NMFTs on the nanofiber array. In these images the cells are not visible because the excitation wavelength for the FRET pair used is higher than the absorption spectrum of calcein. The FRET images shows donor excitation and emission on the left, and donor excitation and acceptor emission on the right.

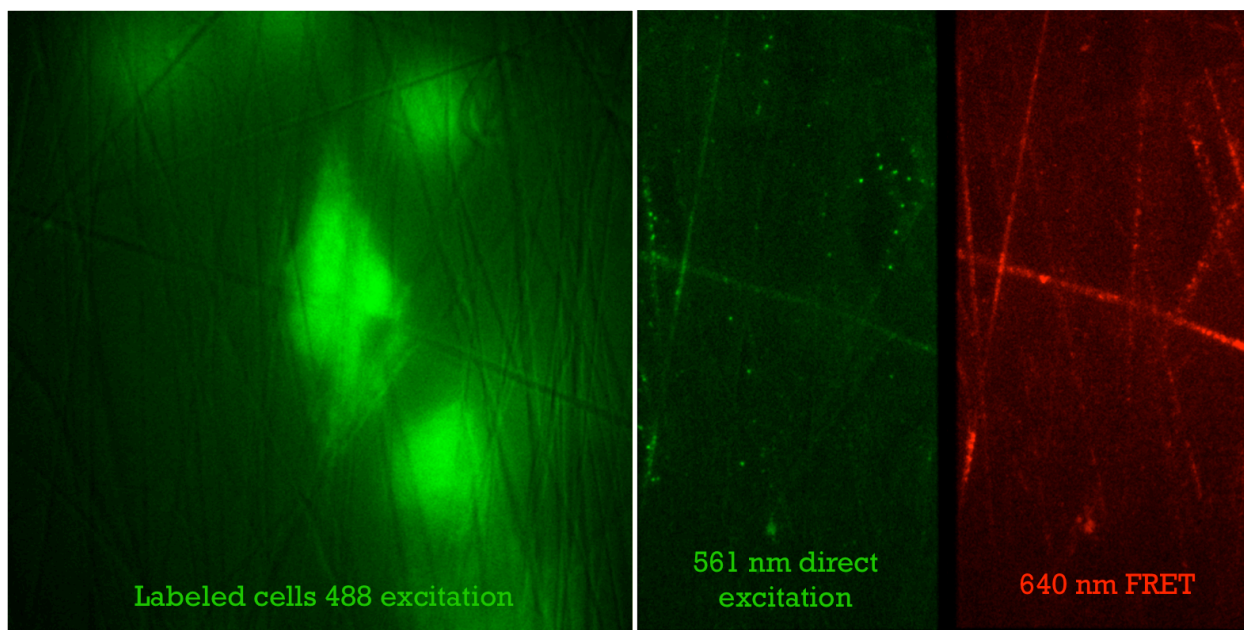


Figure 13 – Cells and NMFTs on electrospun nanofiber array

### Future Work and Impact

The next steps in the research will be first to calibrate the force/FRET behavior of the NMFTs. NMFTs will be calibrated by directly applying controlled forces and measuring the FRET readout as a function of force. A magnetic tweezers device was developed to integrate with our fluorescence microscope. NMFTs will attach to a surface on one end and a magnetic bead on the other. Then, a magnetic field will be introduced to apply a force to the magnetic beads and stretch the NMFTs resulting in a change in FRET efficiency. This magnetic field can be converted into an applied force to validate the force/FRET behavior of the NMFTs given in equation 6.

Once the devices are calibrated, longer time-lapse experiments will be conducted to measure the field of traction forces during cell migration. The field of traction forces of healthy and cancerous cells can be compared and contrasted. Ultimately, we will use the insight gained from NMFT traction force experiments to guide design of nanofiber pathways for separation of

cancerous and healthy cells. These experiments will be performed in collaboration with the Dr. John Lannutti's lab in Ohio State University's Materials Science and Engineering Department. More generally, this research will demonstrate the ability to develop intelligent materials that are capable of sensing their local environment.



## Support/Collaboration

- OSU CANPBD (Center for Affordable Nanoengineering of Polymeric Biomedical Devices)
  - Funded through the National Science Foundation
- Laboratory for Biomolecular Nanotechnology, Technische Universität München
- The Poirier Lab, OSU Department of Physics
- OSU CMIF (Campus Microscopy and Imaging Facility)
- OSU NBL (Nanoengineering and Biodesign Laboratory)

## References

- [1] M Dembo, Y. Wang. “Stresses at the Cell-to-Substrate Interface during Locomotion of Fibroblasts.” *Biophysical Journal* **April 1999**, Vol. 76, 2307-2316
- [2] M Dembo *et al.* “Traction Force Microscopy of Migrating Normal and H-ras Transformed 3T3 Fibroblasts.” *Biophysical Journal* **April 2001**, Vol. 80, 1744-1757
- [3] C. Franck *et al.* “Three-Dimensional Traction Force Microscopy: A New Tool for Quantifying Cell-Matrix Interactions.” *PLoS ONE* **March 2011**, Vol. 6 Issue 3
- [4] A. Ganz *et al.* “Traction forces exerted through N-cadherin contacts.” *Biology of the Cell* **2006**, Vol. 98 No. 12, 721-730
- [5] I Schoen *et al.* “Probing Cellular Traction Forces by Micropillar Arrays: Contribution of Substrate Warping to Pillar Deflection.” *Nano Letters* **2010**, 10, 1823-1830
- [6] P. Rothemund. “Folding DNA to create nanoscale shapes and patterns.” *Nature* **March 2006**, Vol. 440, 297-302
- [7] C. Castro *et al.* “A primer to scaffolded DNA origami.” *Nature Methods* **March 2011**, Vol. 8 No. 3, 221-229
- [8] H. Dietz *et al.* “Folding DNA into Twisted and Curved Nanoscale Shapes.” *Science* **August 2009**, Vol. 325, 725-730
- [9] C. Castro. “Biomechanical structure-function relationships of collagen tissues, B Cell membranes, and amyloid fibers.” *Doctoral dissertation* **2010**, Massachusetts Institute of Technology
- [10] M. Wang *et al.* “Stretching DNA with Optical Tweezers.” *Biophysical Journal* **March 1997**, Vol. 72, 1335-1346